

THEORETICAL AND EXPERIMENTAL INVESTIGATION OF ENERGY EXTRACTION FROM ATMOSPHERIC TURBULENCE

Chinmay K. Patel* , Ilan M. Kroo**

*Acuity Technologies Inc., Menlo Park, CA. **Stanford University, Stanford, CA.

Keywords: *Atmospheric turbulence, Gust soaring, Energy extraction, Control law design*

Abstract

Birds frequently use the energy present in atmospheric currents to conserve their energy while flying. Although energy in the form of thermal updrafts is routinely used by pilots of full-scale and model sailplanes, the energy in atmospheric turbulence has not been utilized to its full potential. This paper deals with the design of simple control laws to extract energy from atmospheric turbulence. A simulation-based optimization procedure to design control laws for energy extraction from realistic turbulence was developed, leading to about 36% average energy savings for a 'bird-sized' glider. Flight test results are presented to demonstrate the energy extraction concept and validate the predicted savings.

1 Introduction

For centuries, observers have been fascinated by the ability of certain birds to fly with little apparent effort. Numerous accounts of birds soaring without flapping their wings, ranging from observations by Leonardo da Vinci to Octave Chanute [1, 2], can be found in literature. Birds circling in thermals or using the ridge lift along a hill or an obstacle are popular examples of advantageous use of atmospheric energy. In addition to thermal convection, birds also exploit the energy from wind shear and random gusts. Albatross, for example, are known to fly very long distances over oceans, without flapping their wings, by extracting energy from the oceanic boundary layer.

The concept of using energy available in the atmosphere has often attracted the attention of aircraft designers and pilots. The energy present in the motion of air, if converted to the energy of an aircraft, could lead to energy savings and improved performance.

Energy from updrafts due to thermals or ridge lift is often used successfully by full-scale and unmanned gliders resulting in tremendous improvements in their capabilities. The flight of albatross in the oceanic boundary layer has been studied by several authors [3, 4, 5, 6]. Dynamic soaring in the shear layer on the leeward side of ridges has become very popular with model aircraft enthusiasts. Proximity to terrain and pilot workload have been the main deterrents in applying such a technique to full-scale sailplanes, along with the fact that wind shear naturally available within atmospheric boundary layer may not be sufficient to provide a significant benefit. The flight speeds of many birds and small Unmanned Aerial Vehicles (UAVs), however, are comparable to atmospheric fluctuations and the energy present in time-dependent atmospheric fluctuations is a much larger fraction of the total power required for flight of these small vehicles.

Energy gain from random wind gusts and turbulence has been studied to some extent but not demonstrated in flight tests [7, 8, 6]. Pilots of hang-gliders and ultralight sailplanes have discovered some of the benefits achievable from carefully controlled flight through gusts [9, 10, 11]. Reduction in the drag of an airplane flying through a vertically fluctuating freestream has

been reported by Katzmyer [12] and Phillips[7, 8]. The use of well-designed control laws could lead to significant energy savings and the possibility of sustained flight using energy extraction techniques. This paper explores the problem of designing simple control laws to extract energy from vertical turbulence. Fig. 1 illustrates how

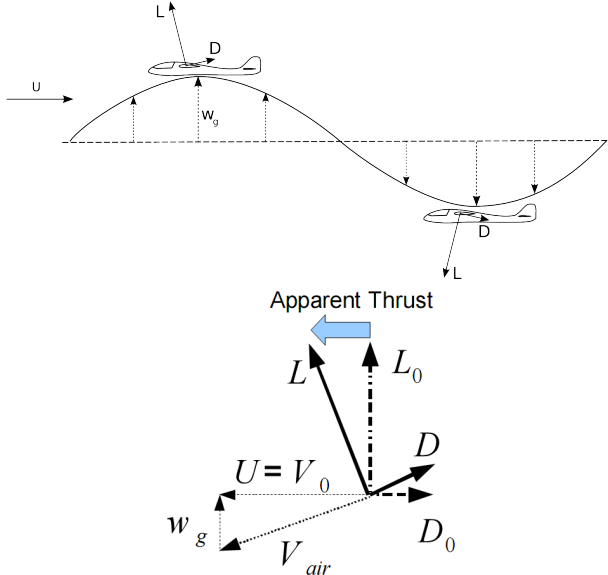


Fig. 1 The fundamental concept of gust soaring.

a component of the lift vector acts as an effective thrust when a glider flies through a vertical gust. The glider flies through a gust of amplitude w_g , at speed U . Vectors L and D denote the lift and drag forces respectively. Since lift acts perpendicular to the local wind, the lift vector is tilted forward and its component acts as an effective thrust. The figure also shows how energy can be gained by flying through a downdraft, by pulling negative g 's. The concept remains valid even if a glider is flying through a lateral gust and the bank angle is such that the glider executes a downwind turn, hence aligning the lift vector with the gust. In general, when the lift vector of an aircraft is aligned such that it has a component in the direction of the atmospheric wind, positive work is done on the aircraft (and negative work on the gust). An alternative argument is that the downwash generated by the glider reduces the magnitude of the gust. In Prandtl's words, "One

must attempt to equalize the fluctuations in the wind" [13].

Earlier work by Lissaman and Patel [14] presented the deterministic case of optimal control laws for neutral energy cycles in sinusoidal vertical gusts. The following sections, which build on the work of Kroo and Patel [15], present a method to determine optimal control laws for energy extraction from random vertical gusts. A description of an autonomous UAV and the results of a flight test demonstration are also presented.

2 Control Law Design

Unlike the deterministic case of a sinusoidal vertical gust, energy extraction from realistic turbulence requires control laws that perform well over a variety of random gusts. Measurements taken at low altitudes in the Earth's boundary layer have shown that the von-Karman or Dryden wind turbulence spectra are representative of natural turbulence [18, 26, 16]. In the present formulation, the 'frozen gust' assumption was used, and the power spectrum of the gust was assumed to follow the Dryden Power Spectral Density (PSD) function. The gusts were modeled as a function of the x (spatial) co-ordinate only. The gust profiles were generated by superposing a set of sinusoids with amplitude corresponding to their relative contribution to the gust intensity and a random phase angle [19].

The aircraft was modeled as a point mass glider flying through a vertical gust. A control law for the coefficient of lift, C_L , was designed to minimize the energy loss as the glider traveled a fixed horizontal distance. Results are shown for gusts generated using the Dryden PSD, and the performance of the optimized control laws is compared over a purely sinusoidal gust. The equations of motion are presented in Eq. 1, where m is the mass of the glider, g the gravitational acceleration, γ the flight path angle, $\{x, z\}$ the horizontal and vertical (positive downwards) components of position, and $\{u, w\}$ the corresponding

components of inertial velocity.

$$\begin{aligned}\frac{du}{dt} &= -\frac{L}{m} \sin \gamma - \frac{D}{m} \cos \gamma \\ \frac{dw}{dt} &= -\frac{L}{m} \cos \gamma + \frac{D}{m} \sin \gamma + g \\ \frac{dx}{dt} &= u \\ \frac{dz}{dt} &= w\end{aligned}\quad (1)$$

The total mechanical energy of the glider per unit mass, with respect to an inertial reference frame, is the sum of its potential and kinetic energy, as shown as H_e in Eq. 2. The initial and final energy states were calculated by integrating the equations of motion of the glider over a 500 m long region of vertical gust.

$$H_e = -gz + \frac{1}{2}(u^2 + w^2) \quad (2)$$

The control law was designed to use the gust velocity, w_g , the glider's airspeed, V_{air} , and a static term to determine the instantaneous C_L of the glider. This C_L can be achieved using several methods, such as flap or elevator deflection, or a change in the wing incidence. For the present study, it was assumed that a mechanism to provide the required C_L exists. Constraints on the maximum lift coefficient, C_{Lmax} , maximum g-load, and the rate of change of C_L were included. A constraint on the rate of change of C_L arises mainly because of actuator bandwidth limitations. Unsteady aerodynamic effects were not significant for the gust frequencies and glider speeds considered here, because the reduced frequencies were sufficiently low (less than 0.1). Post stall behavior can also be modeled, but for the sake of estimating an upper bound on the possible energy savings, it was assumed that the airplane is able to maintain its C_{Lmax} for the duration required. The coefficient of drag, C_D , was modeled as a parabolic drag polar of the form shown in Eq. 3, using the parasitic drag coefficient, C_{Dp} , and the effective aspect ratio, AR_e .

$$C_D = C_{Dp} + \frac{C_L^2}{\pi AR_e} \quad (3)$$

The control law used in the simulations is shown in Eq. 4. The coefficient of lift, C_L , at a particular instant is determined as a function of the gust velocity, the deviation from a reference airspeed, V_{ref} , and a fixed component. The first term in Eq. 4 is directly related to the angle of attack of the glider. The second term is a feedback based on the ratio of the glider's airspeed to the reference airspeed. This term ensures that the airspeed is maintained close to the reference airspeed, and helps regulate the load factor. The feedback gains, K_1 , K_2 , and K_3 , are design variables to be determined using an optimization procedure. Transforming the problem of finding the optimum instantaneous C_L into a problem of finding the optimal gains for various feedback loops makes it amenable to practical implementation. It also reduces the dimensionality of the optimization problem so that evolutionary algorithms may be used. This C_L may be obtained by deflecting one or more of the control surfaces on an aircraft. Results with full-span flaps used to control the C_L of the airplane are presented in Section 3.

$$C_L = K_1 \frac{w_g}{V_{air}} + K_2 \frac{V_{air}}{V_{ref}} + K_3 \quad (4)$$

Fig. 2 illustrates the overall methodology for the

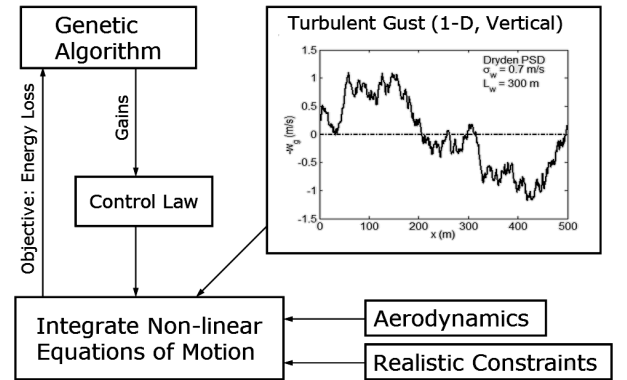


Fig. 2 Overall design methodology.

design of the control law shown in Eq. 4. The feedback gains were determined using a real encoded Genetic Algorithm (GA) that minimized the energy loss computed from a numerical simulation of the glider's flight through a gust. A fourth order Runge-Kutta scheme was used to integrate the non-linear equations of motion.

Most of the relevant literature in this field involves the use of dynamic programming or collocation based methods for trajectory optimization. This is mainly because steady wind gradients and sinusoidal gusts, and not random turbulence, are considered [3, 4, 20, 21, 22, 14, 23]. However, one of the important aspects of energy extraction from random wind turbulence is the stochastic nature of turbulence, which must be included in the design process. The optimized control law should yield good results, on an average, over a wide range of gusts, and should not be tailored to one particular gust profile. This was accomplished in the above procedure by randomly changing the gust profile with every new generation in the GA. This ensured that the surviving members of the population had good performance over several different gusts, by virtue of their ancestry. Once an optimal control law was found, it was tested over a set of random gusts to determine the average energy savings achieved in comparison to an optimized fixed C_L glide through the same set of gusts. Results for small UAVs show that significant energy savings are possible even with simple control laws.

2.1 Results

Using the procedure described in the Section 2, control laws of the form shown in Eq. 4 were designed. The results shown in Fig. 3 and Fig. 4 are based on the parameters listed below for the flight test UAV described in Section 3.

- Mass: $m = 0.475 \text{ kg}$
- Wing Area: $S_{ref} = 0.331 \text{ m}^2$
- Wing span: $b_{ref} = 1.97 \text{ m}$
- Wing aspect ratio: $AR = 11.7$
- Wing mean aerodynamic chord: $\bar{c} = c_{ref} = 0.174 \text{ m}$
- Parasite drag coefficient: $C_{Dp} = 0.023$
- Oswald efficiency: $e = 0.75$
- Reference speed: $V_{ref} = 5.4 \text{ m/s}$ (corresponds to maximum L/D ratio of 17.3)
- Maximum lift coefficient: $C_{Lmax} = 1.2$ (without the use of flaps)

All simulation runs were carried up to a final distance, $x_f = 500 \text{ m}$. Realistic gust profiles were generated using the Dryden PSD (with length scale, $L_w = 300 \text{ m}$, and intensity, $\sigma_w = 0.7 \text{ m/s}$), and the optimized control law found using the optimization procedure is shown in Eq. 5. Fig. 3 shows the variation of the important quantities as the glider traverses a gust generated using the Dryden PSD function.

$$C_L = -2.3811 \frac{w_g}{V_{air}} + 0.1864 \frac{V_{air}}{V_{ref}} + 0.6510 \quad (5)$$

It is seen from Fig. 3 that the C_L increases dur-

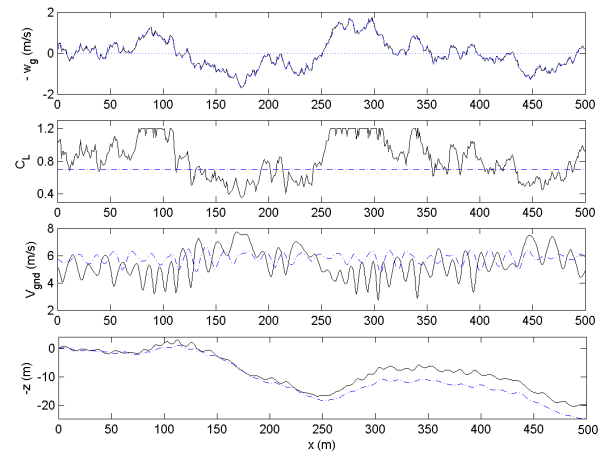


Fig. 3 Optimized control law simulated over a Dryden gust.

ing regions of updraft and decreases in regions of downdraft. This enables the glider to extract energy from the gust by spending more time in an updraft (dolphin soaring), and also from the non-linear effect due to the tilting of the lift vector, resulting in a gain in altitude. The C_{Lmax} constraint is active in certain portions of high upward gust velocity. In regions of downdraft, the C_L is reduced and the glider dives in order to traverse the downdraft in less time. The energy savings, as compared to a glide with an optimized but fixed C_L (represented by blue dotted lines), were found to be 36.07% for gusts generated using the Dryden PSD. Since these gusts are random in nature, the 36.07% reduction in energy loss reported here is the average reduction over 50 random Dryden gusts, using the optimized control law shown in

Eq. 5. The active control law performed better than a fixed C_L glide on each of the 50 random gusts. The control law shown in Eq. 5, which was

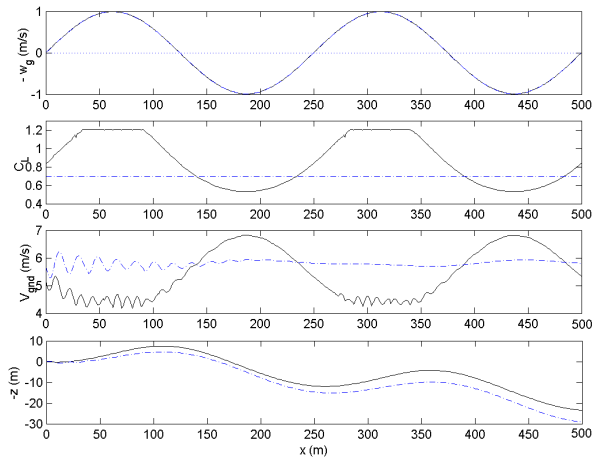


Fig. 4 Optimized control law simulated over a sinusoidal gust with $\lambda = 250$ m.

developed for Dryden gusts, was then used over a low frequency sinusoidal gust of wavelength, $\lambda = 250$ m, for comparison of the energy savings, and to verify the physics behind the control law. The results are shown in Fig. 4. It can be seen that the control law follows the energy extraction technique described in Section 1, and observed in Fig. 3. The energy savings for this gust were 19.42%.

3 Experimental Validation

The concept of energy extraction from wind currents has been known for decades. However, no attempt has successfully demonstrated energy extraction from random gusts using an autonomous UAV. One of the reasons for this is the inability of full-scale aircraft and large UAVs to extract noticeable amounts of energy from natural turbulence. However, ‘bird-sized’ UAVs have low power requirements and can benefit from atmospheric energy. Hence, it was decided to verify some of the results obtained from the simulations described in Section 2, and to demonstrate the feasibility of the concept using an experimental test-bed. To this effect, a small UAV and a lightweight autopilot were designed, built, and

test flown at Stanford University. An overview of the autopilot and the UAV is provided in this section. Results related to the performance of the UAV, the autopilot, and the control laws are discussed.

For the purposes of experimental validation, the UAV was test flown with active control implemented in the longitudinal axis. The flight test procedure was designed to reduce the effect of lateral dynamics.

3.1 Design of the Autopilot

A low-cost, lightweight autopilot board was designed for the purposes of research within the Aircraft Aerodynamics and Design Group and UAV design course-work at Stanford University. The intensity of turbulence required to obtain significant benefits is directly proportional to the cruise speed of the vehicle [14]. In order to have energy requirements comparable to those of birds, the UAV would have to fly in the 5.0-10.0 m/s range. It was evident that sensors with adequate resolution in this speed range were required. The sensors used with this autopilot were chosen to be accurate for small and slow flying UAVs. A block diagram of the autopilot is shown in Fig. 5, and its specifications are listed below.

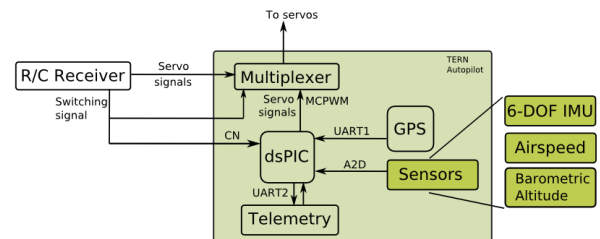


Fig. 5 A block diagram of autopilot components.

- 29.49 MHz micro-controller
- GPS module with 4 Hz update rate
- 6-axis Inertial Measurement Unit (IMU)
- Airspeed sensor with 2.5 cm/s resolution in the 0-20.0 m/s range
- Barometric altitude sensor with 60 cm resolution in the 0-575 m range

- Two-way wireless communication link with 1 mile range
- Built-in servo PWM signal generator
- Built-in manual override capability for four servo channels
- Mass: 65.0 gm (including the pitot tube, battery pack, and wiring)
- Size: 5.08 x 6.35 x 3.20 cm

Fig. 6 shows an image of the UAV system, including the ground station. An attitude estima-



Fig. 6 The UAV system, including the ground station.

tion algorithm based on an Extended Kalman Filter (EKF) and a total energy estimation algorithm were implemented in the autopilot to enable autonomous flights with precise and rapid feedback control. Details about the algorithms can be found in references [16] and [17].

It was found during flight testing that accurate estimation of the gust velocity was not possible due to hardware and computing power limitations. However, knowledge of the true gust velocity was not expected to be necessary. The effects of gust velocity on the glider were used to implement the feedback control laws. The expression for the total energy of the glider is shown in Eq. 6. Note that this expression for total energy is not with respect to an inertial frame of reference because the airspeed of the airplane is used to compute its energy. However, it does provide an estimate of the energy state of the vehicle.

$$E = mgh + \frac{1}{2}mV_{air}^2 \quad (6)$$

The rate of change of the energy, \dot{E} , is often interpreted by sailplane pilots as the strength of the

vertical component of wind, and has been used in recent work on autonomous soaring [24]. Simulations of a glider flying through a vertical gust field show that \dot{E} follows the gust velocity very closely [16]. Hence, it was decided to use \dot{E} as one of the feedback loops in the control laws designed for active control instead of the gust velocity, w_g . The barometric altitude and airspeed sensors were used in determining the total energy, E , of the airplane. Since direct differentiation of E would lead to a very noisy estimate of \dot{E} , a Kalman Filter was used to estimate E , \dot{E} and \ddot{E} from sensor measurements. These ‘variometer’ estimates were then used as an input to the energy extraction algorithm, as a surrogate for the vertical gust velocity.

3.2 Description of the UAV

The size of the UAV was determined mainly by the size and weight of the autopilot system. A low wing-loading was necessary in order to lower the power requirements for flight and increase the observable energy gain. The UAV was designed to be relatively clean, and airfoils with low drag coefficients at high speeds were chosen to provide a large speed range. The wing aspect ratio was chosen as a compromise between the induced drag and low Reynolds number effects on parasite drag. The all-up weight of the autonomous UAV was 475 gm. A brushless motor and a folding propeller were used as a propulsion system for positioning and retrieving the aircraft after a test run. The powerplant was turned off during energy extraction tests, with the folding propeller making sure the drag penalty due to the propulsion system was minimal. Full span flaperons were provided to enable the autopilot to rapidly change the camber of the entire wing making it possible to implement the control laws described in Section 2.

The mass properties of the UAV, required for the design of control laws, were determined by measuring the time period of oscillation about the three body axes, assumed to be the principal axes. The aerodynamic characteristics of the UAV were estimated using *LinAir 4*, a discrete

vortex method for analysis of multiple lifting surfaces [25]. These mass properties and stability derivatives were used in simulations for control law design.

3.3 Flight Test Results

Several hours worth of flight tests were conducted to calibrate the sensors on the autopilot and determine the characteristics of the UAV. Basic tasks such as bank angle and heading hold, airspeed hold, and waypoint navigation were successfully completed in the process.

3.3.1 Turbulent Gusts Experienced by the UAV

Very little empirical data on gusts experienced by small UAVs are available in literature. The Dryden and von-Karman PSD spectra were developed mainly to characterize turbulence encountered by full-scale aircraft. These spectra ignore the effects of terrain features, convection, lapse rate, and cross-correlation between components of turbulence. Although this research did not focus on collecting a large amount of data to establish a turbulence model for small UAVs, some flights were performed with the goal of collecting gust data. The rate of change of energy, \dot{E} was used as a surrogate for the gust velocity. Since the altitude change as well as airspeed change contribute to \dot{E} , longitudinal and vertical gust components were captured. The motion of the airplane due to the gust was accounted for in the measured \dot{E} .

Fig. 7 shows a comparison of the PSD of \dot{E} logged on a moderately gusty day, with the airplane facing upwind with near zero ground speed at an altitude of approximately 150 m Above Ground Level (AGL). The slope of the PSD of \dot{E} matches well with the Dryden PSD. This result is in agreement with recent results obtained by Watkins et. al for the von-Karman spectrum [18, 26]. It was observed from several such plots that the empirical PSD curve showed a larger contribution from low frequency gusts, as compared to the Dryden PSD curve. For frequencies higher than 1 cycle/m, the flight logged PSD curve showed a slope of slightly less than -2. The

data collected in this research agree qualitatively with existing turbulence models, but additional data on turbulence experienced by small UAVs flying within the planetary boundary layer would be very helpful in characterizing the environment small UAVs and birds fly in.

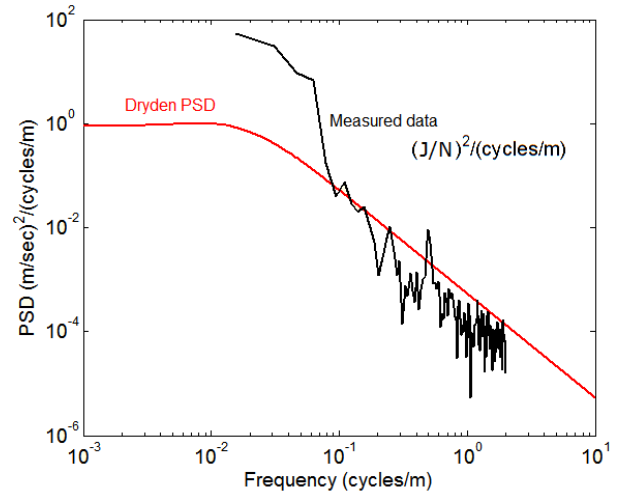


Fig. 7 Comparison of flight test data with the Dryden PSD curve.

3.3.2 Flight Test Procedure for Energy Extraction Flights

As stated earlier, the energy extraction control laws were implemented only in the longitudinal axes. The airplane was flown to an altitude of approximately 125 m under manual control. Once the airplane was trimmed to fly upwind, the throttle was turned off and the autopilot was enabled. The autopilot was programmed to hold the GPS heading at which it was enabled. The region available for flight testing permitted straight glides of 150-200 m range. Once the UAV glided across the available flight test area, it was flown back to the starting position and heading under manual control. Alternate test runs were made with fixed control settings and actively controlled flaps. Full-span flaperons provided a direct means for controlling the lift of the airplane. The flight test data were logged on the ground station and analyzed after each flight.

A schematic for the feedback control loops for flap deflection is presented in Fig. 8. The el-

evator was held fixed during the flight test runs. The control law design procedure was extended to include pitch dynamics resulting from flap deflections. The feedback gains were coarsely determined using simulations and then fine-tuned during flight testing.

$$\delta_f = K_p \dot{E} + K_d \ddot{E} \quad (7)$$

Flights for the energy extraction tests were con-

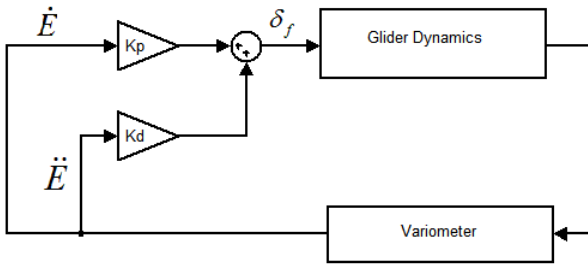


Fig. 8 Schematic of active control of flaps for energy extraction.

ducted in mean winds of 10-15 knots at an average altitude of 100-70 m altitude. Given the low wing loading of the UAV, it was challenging to fly it precisely on gusty days under manual control. However, the autopilot performance was better in such gusty conditions, because of the estimation algorithms and feedback control laws used.

3.3.3 Results

Following the procedure outlined in the previous subsection, several flights were conducted to determine the gain due to energy extraction from turbulence by active control of the flaps. This section presents the data collected from flights conducted on turbulent days with no significant convective activity. At flight test altitudes of about 125 m, the wind speed estimated from flight test data was in the 5.0-6.6 m/s (10-13 knots) range.

The variation of specific total energy, $\Delta E = E/(mg)$, with time for one of the test flights is shown in Fig. 9. Each curve in these figures represents one straight and level glide. The black curves represent glides with fixed control surfaces. The flaps were actuated according to the

control law shown in Eq. 7 on alternate test runs. These ‘soaring’ runs are indicated as red curves in Fig. 9. Further data from flight tests are available in references [16] and [17]. The follow-

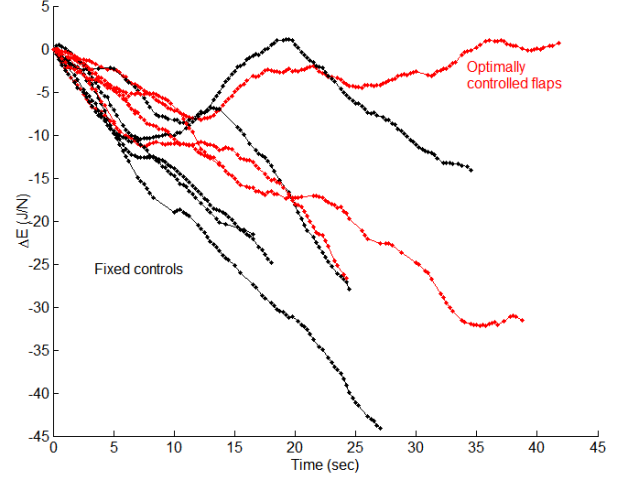


Fig. 9 Flight test data.

ing observations can be made from the flight test data:

- The plots of ΔE versus time show significant variation. This is to be expected because of the stochastic nature of the gusts. No two gusts encountered by the UAV are expected to be identical. Because of the effects of convective activity and terrain features, the nature of gusts found in the same spatial region may vary with time. This results in the variation seen in flight test data. Based on visual observation, one can say that the red curves representing active control of flaps are often higher than the ones with fixed controls glides. However, there are situations when the glider loses more energy using the active control law, as compared to a fixed controls run during the same flight. This is also the result of the stochastic nature of turbulence, and highlights the need for designing robust control laws suitable for a wide variety of gusts.
- Energy gain is observed in some portions of the black curves, which represent test runs with fixed control surfaces. When an

aircraft flies through a gust with fixed control surfaces, its angle of attack changes because of the influence of the gust. This results in a change of the lift vector, which leads to average energy savings. This phenomenon was analyzed by Phillips [7], and is similar to the Katzmyer effect observed in airfoils in oscillating freestream flow [12].

- The test runs with active control are often longer than the ones with fixed controls. Since the flight test runs were initiated at a fixed altitude of approximately 125 m, a significant loss of altitude brought the UAV close to trees present on the testing site. If the pilot determined that the altitude was not enough to safely recover in the event of autopilot malfunction, the test run was terminated and the autopilot was disengaged. The actively controlled glides led to a smaller rate of descent leading to longer test runs.

Although most of the actively controlled test runs resulted in a net loss of energy, there were cases in which the glider traveled a distance of 150-200 m without any loss of energy. In one of the runs, the glider gained approximately 20 m in altitude at the end of a ‘soaring’ run without losing its airspeed. These observations reinforce the claim that natural turbulence, with an intensity of 10-15% of the vehicle’s cruise speed, is sufficient to sustain flight for small UAVs using simple control laws and conventional sensors and control surfaces.

Flight test results from 13 fixed controls test runs and 15 ‘soaring’ runs, with optimal control of flaps, are presented here. In order to statistically analyze this data, each flight test run was divided into 10 second segments, leading to 34 fixed controls samples and 61 optimal control samples. Table 1 lists the average savings based on these flight tests and shows that the optimal control test runs lead to 46.22% energy savings on average. The ‘soaring’ runs also show better performance when the median, best and worst samples are compared. The percentage of

samples with a given energy loss are plotted in Fig. 10 for both types of test runs. The curves show that the red samples, representing active control of flaps, are consistently better than the samples with fixed control surfaces. Approximately 19.0% of the ‘soaring’ samples show zero energy loss, as opposed to only 6.0% of the fixed controls samples. The mean and $2 - \sigma$ confidence

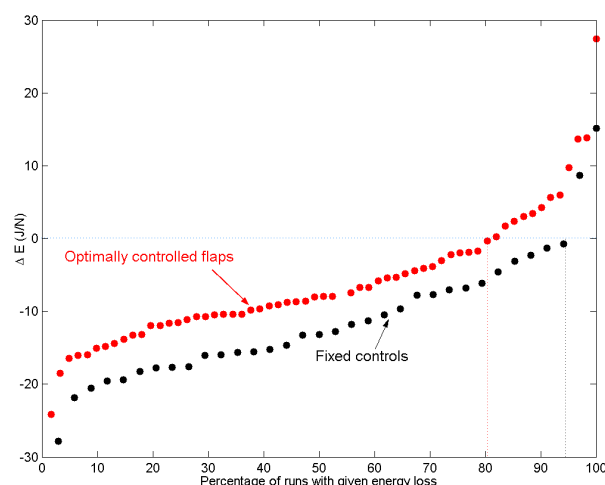


Fig. 10 Effect of active control of flaps on energy loss.

intervals of the data collected from fixed control and optimal control runs are shown in Fig. 11. On an average, the fixed controls and optimally controlled test runs both lead to a net energy loss. It is seen that the $2 - \sigma$ bands, representing the uncertainty in the mean, have negligible overlap. Hence, it is concluded that the optimally controlled runs lead to higher average energy savings with a high probability.

4 Conclusions

The theoretical results presented in Section 2 show that significant energy savings are possible, even with the simple feedback control law shown in Eq. 4. Average energy savings of 36.07% were computed for a small UAV using an optimal control law designed for energy extraction from random turbulent gusts.

A capable, lightweight, and low-cost autopilot was designed as a part of this research. An instrumented UAV was built and test flown in order

$\Delta E(J/N)$	Fixed controls	Optimally controlled flaps	% improvement
Mean	-11.17	-6.00	46.22
Median	-12.99	-7.98	38.56
Best sample	15.14	27.40	80.97
Worst sample	-27.86	-24.12	13.42

Table 1 Statistical analysis of flight test data.

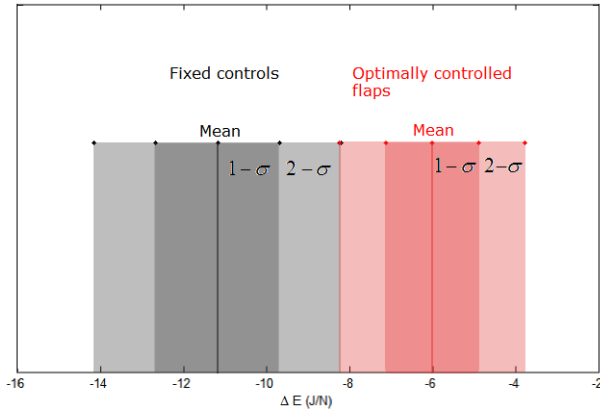


Fig. 11 Comparison of mean and $2 - \sigma$ confidence intervals of flight test data.

to demonstrate the feasibility of energy extraction from atmospheric turbulence. A flight test procedure was developed to determine the energy savings due to optimal control. Flight tests suggest that the PSD of gusts experienced by the UAV match the slope of the Dryden spectrum.

Average energy savings of 46.22% were observed in flight tests conducted using full-span flaperons for changing the lift of the aircraft. Approximately 19.0% of the samples with active control resulted in no energy loss. The stochastic nature of the problem, arising due to the randomness of natural gusts, is evident from the variation in flight data. To account for this uncertainty, the mean and $2 - \sigma$ confidence intervals of the mean value were compared. The flight test results clearly demonstrate the feasibility of the concept of energy extraction from atmospheric turbulence, even with very simple feedback control laws implemented on existing control surfaces.

References

- [1] W. J. Jackman and T. H. Russell. *Flying machines: construction and operation*. Chapter XX, The Charles C. Thompson Co., Chicago, USA, 1910.
- [2] D. Laurenza. *Leonardo on flight*. Giunti Press, Milan, Italy.
- [3] G. Sachs and O. da Costa. Optimization of dynamic soaring at ridges. AIAA paper 2003–5303, August 2003.
- [4] G. Sachs. Minimum shear wind strength required for dynamic soaring of albatrosses. *IBIS*, 147, 2005.
- [5] P. B. S. Lissaman. Wind energy extraction by birds and flight vehicles. AIAA paper 2005–241, January 2005.
- [6] F. Hendriks. *Dynamic soaring*. Ph.D. Thesis, University of California, Los Angeles, Los Angeles, 1972.
- [7] W. H. Phillips. Propulsive effects due to flight through turbulence. *Journal of Aircraft*, 12(7):624–626, 1975.
- [8] N. de Divitiis. Effect of microlift force on the performance of ultralight aircraft. *Journal of Aircraft*, 39(2):318–325, 2002.
- [9] P. Ciotti. A little lift. *Smithsonian Air&Space Magazine*, April-May, pages 58–63, 2005.
- [10] T. Kicenuik. Dynamic soaring and sailplane energetics. *Technical Soaring*, 25(4), 2001.
- [11] T. Kicenuik. Calculations on soaring sink. *Technical Soaring*, 25(4), 2001.
- [12] R. Katzmyer. Effect of periodic changes in angle of attack on behavior of airfoils. NACA-TM-147, 1922.
- [13] L. Prandtl. Some remarks concerning soaring flight. NACA-TM-47, October 1921.
- [14] C. K. Patel and P. B. S. Lissaman. Neutral energy cycles for a vehicle in sinusoidal and tur-

- bulent vertical gusts. AIAA paper 2007–863, January 2007.
- [15] C. K. Patel and I. M. Kroo. Control law design for improving uav performance using wind turbulence. AIAA paper 2006–231, January 2006.
- [16] C. K. Patel. *Energy extraction from atmospheric turbulence to improve flight vehicle performance*. Ph.D. Thesis, Stanford University, Stanford, CA, 2007.
- [17] C. K. Patel. *Energy extraction from atmospheric turbulence to improve aircraft performance*. VDM Verlag, Germany, 2008.
- [18] S. Watkins and G. Vio. The turbulent wind environment of birds, insects and MAVs. 15th Australasian fluid mechanics conference, December 2004.
- [19] F. M. Hoblit. *Gust Loads on Aircraft: Concepts and Applications*. AIAA Education Series, 1988.
- [20] B. L. Pierson and J. L. de Jong. Cross-country sailplane flight as a dynamic optimization problem. *International Journal for Numerical Methods in Engineering*, 12, 1978.
- [21] B. L. Pierson and I. Chen. Minimum altitude-loss soaring in a sinusoidal vertical wind distribution. *Optimal Control Applications & Methods*, 1, 1980.
- [22] Y. J. Zhao and Y. C. Qi. Minimum fuel powered dynamic soaring of unmanned aerial vehicles utilizing wind gradients. *Optimal Control Applications and Methods*, 25, 2004.
- [23] J. L. de Jong. Instationary dolphin flight: The optimal energy exchange between a sailplane and vertical currents in the atmosphere. *Optimal Control Applications and Methods*, 6:113–124, 1985.
- [24] M. J. Allen. Guidance and control of an autonomous soaring vehicle with flight test results. AIAA paper 2007–867, January 2007.
- [25] LinAir 4. Desktop Aeronautics, Palo Alto, CA.
- [26] B. J. Loxton, S. Watkins, J. Milbank and W. H. Melbourne. Atmospheric winds and their implications for microair vehicles. *AIAA Journal*, 44(11):2591–2600, 2006.

institution, hold copyright on all of the original material included in their paper. They also confirm they have obtained permission, from the copyright holder of any third party material included in their paper, to publish it as part of their paper. The authors grant full permission for the publication and distribution of their paper as part of the ICAS2008 proceedings or as individual off-prints from the proceedings.

Copyright Statement

The authors confirm that they, and/or their company or